Available online at www.sciencedirect.com
ScienceDirect
Journal of Molecular Spectroscopy 245 (2007) 34–51
Journal of MOLECULAR SPECTROSCOPY
www.elsevier.com/locate/jms

Line shape parameters measurement and computations for self-broadened carbon dioxide transitions in the 30012 ← 00001 and 30013 ← 00001 bands, line mixing, and speed dependence

A. Predoi-Cross [a,*], A.V. Unni [a], W. Liu [a], I. Schofield [a], C. Holladay [a], A.R.W. McKellar [b], D. Hurtmans [c]

[a] Physics Department, University of Lethbridge, 4401 University Drive, Lethbridge, AB, Canada T1K 3M4
[b] Steacie Institute for Molecular Sciences, National Research Council of Canada, Ottawa, ON, Canada K1A 0R6
[c] Service de Chimie Quantique et Photophysique, Université Libre de Bruxelles, 50 Av F.D. Roosevelt, cp160/09, B-1050 Bruxelles, Belgium

Received 24 May 2007; in revised form 29 June 2007
Available online 28 July 2007

Abstract

Transitions of pure carbon dioxide have been measured using a Fourier transform spectrometer in the 30012 ← 00001 and 30013 ← 00001 vibrational bands. The room temperature spectra, recorded at a resolution of 0.008 cm^{-1}, were analyzed using the Voigt model and a Speed Dependent Voigt line shape model that includes a pressure dependent narrowing parameter. Intensities, self-induced pressure broadening, shifts, and weak line mixing coefficients are determined. The results obtained are consistent with other studies in addition to the theoretically calculated values. Exponential Power Gap (EPG) and Energy Corrected Sudden (ECS) scaling laws were used to calculate the relaxation matrix elements.

Keywords: Carbon dioxide; Line shapes; Self-broadening; Self-line mixing; Self-shift; Fourier transform infrared spectroscopy (FTIR)

1. Introduction

The limited spectral resolution of early spectrometers was not enough to unveil the fine details of spectral line shapes and most observations reported only line width results. The early theoretical line shape studies [1–6] related the line widths to molecular collisional relaxation processes and molecular velocities—processes assumed to be uncorrelated.

The most commonly used spectral line shapes are the Gaussian, Lorentzian, and Voigt profiles but these models are not comprehensive enough to explain the details obtained from high-resolution spectra. For many years the Voigt profile was considered to reproduce the spectral lines over a wide range of pressures. More complex models developed recently [7–12] account for line mixing effects, speed-dependent profiles, and the correlation between the relaxation of the internal and translational motion of the molecules. High-quality spectral information is particularly important to substantiate these present models and is necessary to develop a fully numerical solution to the formal theory.

An accurate analysis of the spectral parameters of carbon dioxide (CO_2) is of interest to the study of remote sensing and its application to the management of greenhouse gases. Carbon dioxide is one of the most abundant greenhouse gas within the atmosphere and is chemically unreactive with a relatively long lifetime of approximately a century. The primary sources and sinks of atmospheric CO_2 are located within the boundary layer near the earth's surface and represent the highest variability of this otherwise relatively well mixed gas. Accurate measurements of these sources, sinks, and also the balance of fluxes is funda-

* Corresponding author. Fax: +1 403 329 2057.
E-mail address: Adriana.predoicross@uleth.ca (A. Predoi-Cross).

0022-2852/$ - see front matter © 2007 Elsevier Inc. All rights reserved.
doi:10.1016/j.jms.2007.07.004

mental towards CO_2 management and the development of high-performance remote sensing techniques.

In the context of global warming, the increase of global average land-surface and sea-surface temperatures have been predominately attributed to anthropogenic and natural changes in the radiative forcing. A recorded increase of radiative forcing is largely due to the anthropogenic influence of increased greenhouse gases concentrations. These gases include CO_2, CH_4, N_2O, and halocarbons with CO_2 representing 60% of the radiative forcing leaving CO_2 as the single most important anthropogenic greenhouse gas.

New global networks of up-looking ground-based Fourier transform spectrometers are being set up to record atmospheric spectra on a long term basis to exploit the advantages of near-infrared wavelengths. The measurement of the atmospheric CO_2 from satellites will also greatly improve all aspects of our understanding of carbon cycle based research. The primary impact these data will have is to "fill in" the sparse and uneven ground-based global atmospheric sampling networks. The orbiting carbon observatory (OCO) mission intends to obtain total column CO_2 measurements with a precision of ~0.3%. It is our hope that the quality of our measurement results will support the science of the global carbon cycle and the OCO mission.

In the spectral range covered by our study the sun's output is near-maximum whereas the thermal emission from the ground is relatively small which consequently allows for a very high signal to noise ratio for atmospheric remote sensing applications. Compared with the visible spectral range, this spectral range offers little interference from other atmospheric species.

The spectral parameters reported here (pertaining to pure CO_2) are relevant for the future remote sensing studies of Mars and Venus whose atmospheres are almost entirely CO_2 gas [13,14]. This application will require accurate knowledge of spectral parameters in a wide range of pressures and temperatures. Our pure gas study presented here is antecedent to a mixed gas study to be published shortly which will be strictly applicable to the Earth's atmosphere.

The two vibrational bands discussed here are part of the Fermi tetrad ($30014 \leftarrow 00001$, $30013 \leftarrow 00001$, $30012 \leftarrow 00001$, $30011 \leftarrow 00001$). Alternate labels for the bands are $(3001)_{III} \leftarrow (000)$ for the $30013 \leftarrow 00001$ band and $(3001)_{II} \leftarrow (000)$ for the $30012 \leftarrow 00001$ band. The first studies of line parameters in both the $30012 \leftarrow 00001$ and $30013 \leftarrow 00001$ bands were reported in 1978 by Suarez and Valero [15,16]. Absolute intensities, self-broadening coefficients, and foreign-gas broadening by Ar and N_2 were measured [15] at temperatures of 197, 233, and 294 K for the $30012 \leftarrow 00001$ band of CO_2 at 6348 cm^{-1}. The intensity parameters and total band intensity were also calculated. In Ref. [16] the authors measured intensities, self-broadening coefficients, and foreign-gas broadening coefficients for Ar and N_2 for transitions in the $30013 \leftarrow 00001$ band of CO_2 at 6228 cm^{-1}. The experiments were carried out at temperatures between 197 and 294 K. The purely vibrational transition moment, Herman–Wallis factors, and total band intensities were determined at different temperatures.

Using a distributed feed back diode laser De Rosa et al. [17] reported pressure induced self-broadening and shift coefficients for 10 transitions (P(20) to P(2)) in the $30012 \leftarrow 00001$ band. N_2- and O_2-broadening and shift have been measured for the most intense lines. Henningsen and Simonsen [18] have measured line strengths, collision-broadening parameters, and pressure shifts. The strengths were modeled with a third-order Herman–Wallis expansion. The line parameters (positions, intensities, air- and self-broadened half-widths, and coefficients of temperature dependence of air-broadened half-widths) for transitions in our bands of interest are also available through the CDSD-1000 database—the high-temperature carbon dioxide spectroscopic databank described in Ref. [19].

Line positions for the $30012 \leftarrow 00001$ and $30013 \leftarrow 00001$ carbon dioxide bands accurate to 2×10^{-5} cm^{-1} have been published previously in Ref. [20] and incorporated into the HITRAN database [21]. A similar study [22] provided line positions for $^{16}O^{13}C^{16}O$ and $^{16}O^{13}C^{18}O$ accurate to better than 1×10^{-4} cm^{-1}. Most of the early intensity measurements available through the CDSD-1000 [19] and HITRAN [21] show uncertainties of 3–5%, making them unsuitable for highly accurate remote sensing retrievals (such as the ones proposed by the OCO mission, for example). A very comprehensive study of the rovibrational bands located between 4550 and 7000 cm^{-1} using the Voigt profile was reported in Refs. [29] and [30]. Few previous studies have addressed the self-broadening and pressure shifting in the $30012 \leftarrow 00001$ and $30013 \leftarrow 00001$ bands. Other than those mentioned in Refs. [29] and [30], recently N_2-, O_2-, He-, Ne-, Ar-, Kr-, and Xe-broadening of five transitions (R(0), P(8)–P(38)) in the $30013 \leftarrow 00001$ band were studied by Nakamichi et al. [26] using cavity ringdown spectroscopy at temperatures between 263 and 326 K. The measured absorption profiles were analyzed with Voigt functions. The diode laser study of Hikida et al. [24] reported self-broadening and intensities retrieved with a Galatry profile for 11 transitions between P(28) and R(28) in the $30013 \leftarrow 00001$ band. A second study by Hikida et al. [25] reported N_2- and O_2-broadening coefficients and computed the air-broadening coefficients for 10 transitions in the $30013 \leftarrow 00001$ band. As in Ref. [24], the spectra were recorded using a near-infrared diode laser spectrometer and analyzed using the Galatry profile.

A diode laser spectrometer was used by Pouchet et al. [23] to measure absolute intensities and N_2- and O_2-broadening for 13 transitions (between R(6) and R(30)) in the $30013 \leftarrow 00001$ band. A comprehensive study of line intensities of four bands for CO_2, around 1.6 and 2.0 μm, was published by Régalia-Jarlot et al. [27]. The measurements were done by implementing both a high-resolution Connes-type Fourier transform spectrometer and a tunable diode laser spectrometer equipped with several telecommunication-type semiconductor laser devices.

Using Fourier transform spectra and a multi-spectrum fitting procedure, Boudjaadar et al. [28] measured absolute line intensities of CO_2 transitions near 1.6 μm, for the three cold bands $30014 \leftarrow 00001$, $30013 \leftarrow 00001$, and $30012 \leftarrow 00001$, and for the two hot bands $31113 \leftarrow 01101$ and $31112 \leftarrow 01101$. Accuracies are on the average 3% and 5% for cold and hot bands, respectively. The authors reported vibrational transition dipole moments and Herman–Wallis coefficients for each band.

Line positions and strengths of carbon dioxide transitions between 4550 and 7000 cm^{-1} were measured by Toth et al. [29] using absorption spectra recorded at 0.01–0.013 cm^{-1} resolution. Forty-two room temperature laboratory spectra were used in the retrievals of line parameters with the Voigt profile. In all, band strengths and Herman–Wallis-like *F*-factor coefficients were determined for 58 (34 of them never reported before) vibration–rotation bands. In a second publication, Toth et al. [30] report the self-broadened width and self-induced pressure shift coefficients for transitions between 4550 and 7000 cm^{-1}.

The $30012 \leftarrow 00001$ and $30013 \leftarrow 00001$ vibrational bands studied here have been discussed in great detail in two recent studies [31,32]. There are indeed similarities between our study and Refs. [31] and [32]. Both studies have used the Speed Dependent Voigt profile with an asymmetric component due to line mixing. However, Refs. [31] and [32] present a constrained multi-spectrum analysis where the line mixing effects are quantified through off-diagonal line mixing coefficients. In this approach the multi-spectrum non-linear least squares retrieval technique was modified to adjust the rovibrational constants and intensity parameters, including Herman–Wallis terms, rather than retrieving the individual positions and intensities. The authors used Speed Dependent Voigt line shapes with line mixing to fit the line profiles. Our paper presents the intensities, pressure induced self-broadening, shift, and weak line mixing coefficients for lines from P(56) to R(54) in the $30012 \leftarrow 00001$ and $30013 \leftarrow 00001$ bands. The line mixing coefficients are measured directly from the spectra using the Voigt and Speed Dependent Voigt line profiles and a multi-spectrum analysis. The self-broadening and self-line mixing coefficients for the two bands have been modeled using the Energy Power Gap (EPG) and Energy Corrected Sudden (ECS) scaling laws.

Fig. 1 is an overview of the carbon dioxide spectrum in the (a) $30013 \leftarrow 00001$ and (b) $30012 \leftarrow 00001$ bands recorded at a pressure of 300 torr and a path of 40 m. These $\Sigma \leftarrow \Sigma$ parallel bands consist of P(J'') and R(J'') branch transitions, and only even J'' levels exist due to nuclear spin statistics for the indistinguishable ^{16}O nuclei. Usually, the experimental spectra are fitted to a Lorentz or a Voigt profile to retrieve the line parameters but these two line shape models may not be able to reproduce the actual absorption profile for a single line. As the pressure increases, the rate of collisions between the molecules increases randomizing the molecular motion into different directions. This reduces the average speed of the molecules producing a narrowing effect in the actual line shape. The Voigt or Lorentzian line shapes alone do not consider this effect. For these reasons we have used a multi-spectrum non-linear least-square fitting program [33] that employed both the Voigt and Speed Dependent Voigt models.

2. Experimental details

All 18 pure carbon dioxide spectra used in the study were recorded at resolutions of 0.008 or 0.009 cm^{-1} (defined as the inverse of the maximum optical path difference) using a Bomem DA3.002 Fourier transform spectrometer at the Steacie Institute for Molecular Sciences at NRC Ottawa. For each measurement 32 scans were co-added to achieve a good signal to noise ratio. Spectra were recorded over a wide range of pressures varying from 8.3 to 701.5 torr. A white-type multiple-traversal cell with a base length of 500 cm [34,35] was used to obtain pathlengths between 40.15 and 80.15 m. The output from the cell was recorded with a germanium detector operated at room temperature. The entire transfer optics was kept under vacuum to make sure that there was no absorption from other impurities. The pressure was measured with two Baratron 127 capacitance manometers with full scale ranges of 10 and 1000 torr. For further verification, the pressure measurement was supplemented with a Wallace and Tiernan precision Bourdon tube gauge, model FA145. Gas pressures were measured to an accuracy of 0.1 torr with an error approaching 0.15% of the full scale range, that is, ±1.5 torr for most spectra (as specified in the Baratron product manual). All the spectra were recorded at room temperature. Lakeshore PT-103 platinum resistance thermometers and Lakeshore Model 91C and Model 211 read out units were used to record temperature with an accuracy of ±0.2 K. A summary of the experimental conditions for all spectra is presented in Table 1.

3. Spectroscopic analysis and discussion of results

The line parameters for pure carbon dioxide transitions were retrieved by a multi-spectrum non-linear least-square curve fitting program [33]. The multi-spectrum fit software models the spectral lines using the line shape model of choice (Voigt, Galatry, Speed Dependent models) convolved with the instrumental line shape function appropriate for the Bomem instrument. The multi-spectrum fit program makes corrections for interferogram truncation and field of view effects. The instrumental line shape function is implemented as a *sinc* function convolved with the aperture (iris) function; calculated based on the iris diameter, focal length of the collimating lens, maximum optical path difference, and the field of view of the FTS instrument. The spectral backgrounds and zero transmission levels were appropriately modeled. The differences between the experimental spectra and the calculated spectra were minimized by adjusting various line parameters through non-linear least-squares fitting (the Marquardt algorithm).

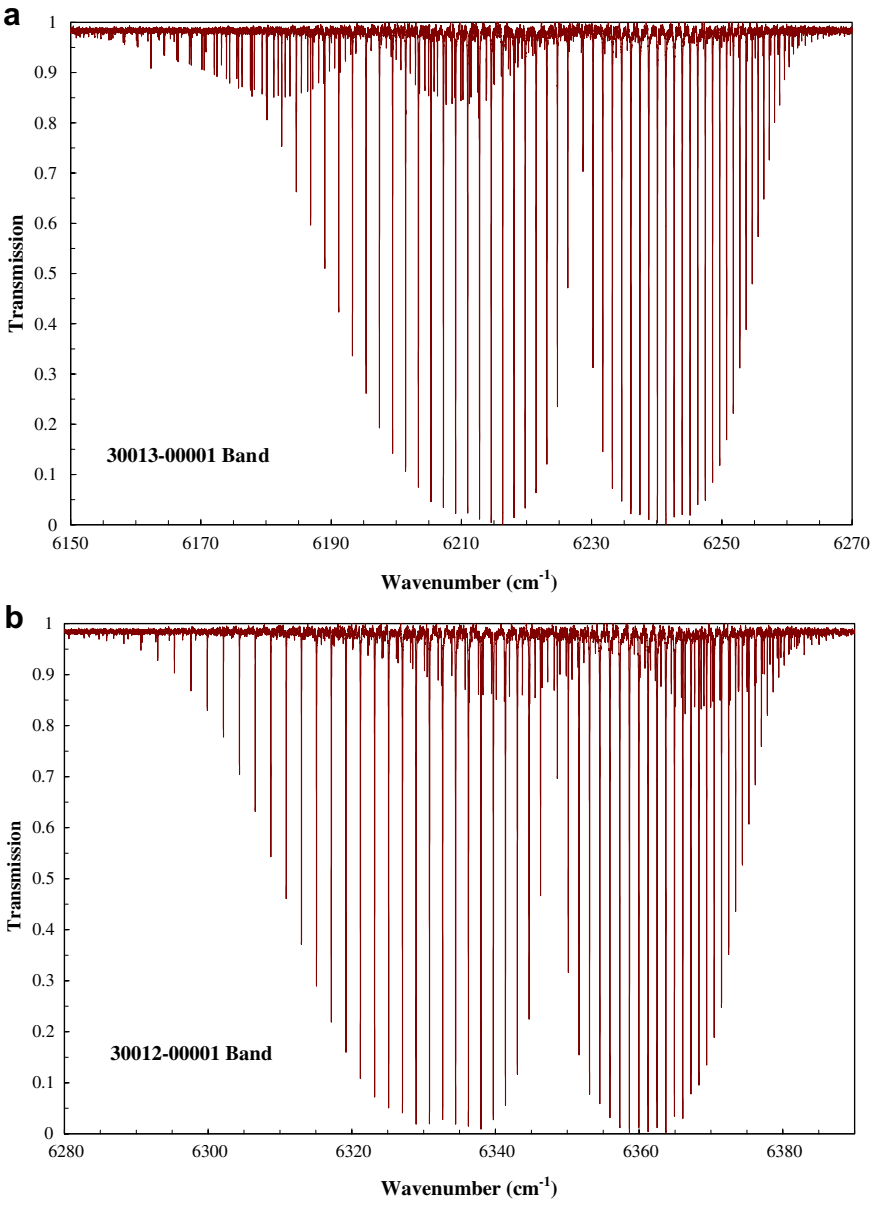

Fig. 1. Overview of the carbon dioxide spectrum of the (a) 30013 ← 00001 and (b) 30012 ← 00001 bands. A gas pressure of 9.5 torr and a pathlength of 40.15 m were used to record the spectra.

The band was analyzed on a line by line basis by selecting the same interval ranging from 1.5 to 3 cm^{-1} within every spectrum. In our analysis using the Voigt profile the initial values for the fit parameters were taken from the study of Toth et al. [30]. Similarly, when we used the Speed Dependent Voigt profile we have used the values from Refs. [30] and [31] as initial guesses. The line positions of the recorded spectra were calibrated internally with respect to the carbon dioxide positions listed in HITRAN 2004 (which are the ones from Ref. [30]). All the spectra recorded on a single day were multiplied by a calibration factor calculated from a low pressure spectrum recorded that day.

A sample of the multi-spectrum fit in the spectral region of the R(8) transition of the 30013 ← 00001 band is presented in Fig. 2. The top panel shows our overlaid spectra of pure carbon dioxide which was used in the multi-spectrum fits. In panels (b) and (c) we show weighted fit residuals from a fit using the Speed-Dependent Voigt profile with a line mixing component and from a fit using the Voigt profile with a line mixing component. Finally, the bottom panel shows our weighted fit residuals from a fit using the Voigt profile. It can be observed that the Speed Dependent line mixing Voigt profile reproduces best our results.

The pressure broadening of spectral lines has been studied for decades now and several mechanisms have been proposed to explain the observed behavior. The Voigt profile, which is widely used by the atmospheric research community, combines the effects of both the thermal motion of

Table 1
Experimental conditions for the pure CO_2 spectra used in our study

Pressure (torr)	Pathlength (m)	Temperature (K)	Resolution (cm^{-1})
8.3	40.15	293.9	0.008
9.5	40.15	293.9	0.008
60	60.15	294.1	0.008
60.2	40.15	294	0.008
99.5	40.15	294.2	0.008
123.7	40.15	293.8	0.008
150.1	80.15	294.2	0.008
200	40.15	293.9	0.008
201	60.15	294.3	0.008
300.5	40.15	294.2	0.008
301	80.15	294.6	0.008
400.6	40.15	294	0.008
501.3	40.15	294.5	0.008
502	60.15	295	0.009
600.3	40.15	294.2	0.008
699	60.15	294.6	0.009
701	60.15	295.1	0.009
701.5	40.15	294.6	0.008

molecules (which leads to a Gaussian (Doppler) line shape) and the effect of molecular collisions (which leads to a Lorentzian line shape). Since the two effects occur simultaneously, the Voigt profile is a convolution of the two broadening mechanisms and can be written as

$$I_v(v) = I_L(v) \otimes I_D(v) = \int_{-\infty}^{\infty} dv' I_L(v - v') I_D(v') \quad (1)$$

where

$$I_L(v) = \left(\frac{\gamma_L}{2\pi}\right) \frac{1}{(v - v_0 - \delta)^2 + \left(\frac{\gamma_L}{2}\right)^2} \quad (2)$$

is the Lorentzian, γ_L is the Lorentzian width, and δ is the pressure shift of the peak of the spectral line with respect to the unperturbed wavenumber v_0 of the line. The Doppler line shape $I_D(v)$ can be expressed as

$$I_D(v) = \frac{2\sqrt{\ln 2}}{\gamma_D \sqrt{\pi}} \exp\left(-4 \ln 2 \frac{(v - v_0)^2}{\gamma_D^2}\right) \quad (3)$$

where

$$\gamma_D = \frac{2v_0}{c} \sqrt{\frac{2k_B T \ln 2}{m_E}} \quad (4)$$

is the Doppler half width, k_B is Boltzmann constant, T is the temperature in K, c is the speed of light, and m_E is the mass of the absorbing molecule.

In a basic theoretical treatment of collisional broadening, the average molecular speed determines the collision rate and the collision cross-section of the active molecules, which in turn determine the collisional broadening, and thus the Lorentzian width. Averaging the molecular speed before determining the width is an approximation. It is more appropriate to divide the molecules into speed classes using a Maxwellian distribution, and then calculate a profile for each class. This approach is still not fully correct, because collisions can change the speed of a molecule, so that it jumps from one class to another. Nonetheless, in practice, the speed-dependent line profiles can account for speed-dependent broadening within the accuracies of this experiment.

In the Speed Dependent Voigt profile, the Lorentzian width γ_L and shift δ are averaged over a Maxwellian velocity distribution for the active molecules [36] as shown in the following equation

$$f_{m_E}(\upsilon_E) = 4\pi \upsilon_E^2 \left(\frac{m_E}{2\pi k_B T}\right)^{3/2} \exp\left(-\frac{m_E \upsilon_E^2}{2k_B T}\right) \quad (5)$$

where υ_E is the velocity of the radiating molecule. The interaction potential is expressed as a power of the intermolecular distance. This leads to a polynomial variation of the pressure broadening cross-sections with the relative speed of the collisional partners. The Speed Dependent Voigt profile can be written in the same form as (1), but with the Lorentzian width γ_L and shift δ in Eq. (2) being replaced by the velocity averaged expressions

$$\gamma_L = \int d\upsilon_{EP} f_\mu(\upsilon_{EP}) \gamma_L(\upsilon_{EP}) \quad (6)$$

and

$$\delta = \int d\upsilon_{EP} f_\mu(\upsilon_{EP}) \delta(\upsilon_{EP}) \quad (7)$$

where $f_\mu(\upsilon_{EP})$ is the same as Eq. (5) but with the mass being replaced by the reduced mass of the active molecule and the perturber. Other implementations of Speed Dependent profiles are described by Pine [37] and Bielski et al. [38].

3.1. Spectral line intensities

The line intensities were modeled as described in detail in Ref. [29]. The transitions studied here belong to the case of $\Delta l = 0$ and $\Delta J = \pm 1$. The line strength, S_v, of an infrared absorption line at wavenumber v may be written as

$$S_v = S_{sb}\left(\frac{v}{v_0}\right) \text{iso} L \left[1 - \exp\left(\frac{-hcv}{k_B T}\right)\right] \frac{\exp\left(\frac{-hcE''}{k_B T}\right) F}{Q_R(T)} \quad (8)$$

where S_{sb} is the sub-band vibrational band strength, v_0 is the center wavenumber of the band, L is the square of the matrix elements of the direction cosine connecting the upper and lower state rotational levels, E'' is the lower state rotational energy, k_B is Boltzmann constant, T is the temperature in Kelvin, F is the Herman–Wallis factor, $Q_R(T)$ is the rotational partition function at temperature T, and iso is the isotopic abundance of $^{12}C^{16}O_2$ in natural samples, equal to 0.9842. The vibrational band strength is given by

$$S_v = g S_{sb} \quad (9)$$

where g is the degeneracy of the rovibrational state. For the 30012 ← 00001 and 30013 ← 00001 bands that have only P and R branches, $g = 1$ and all the transitions have the par-

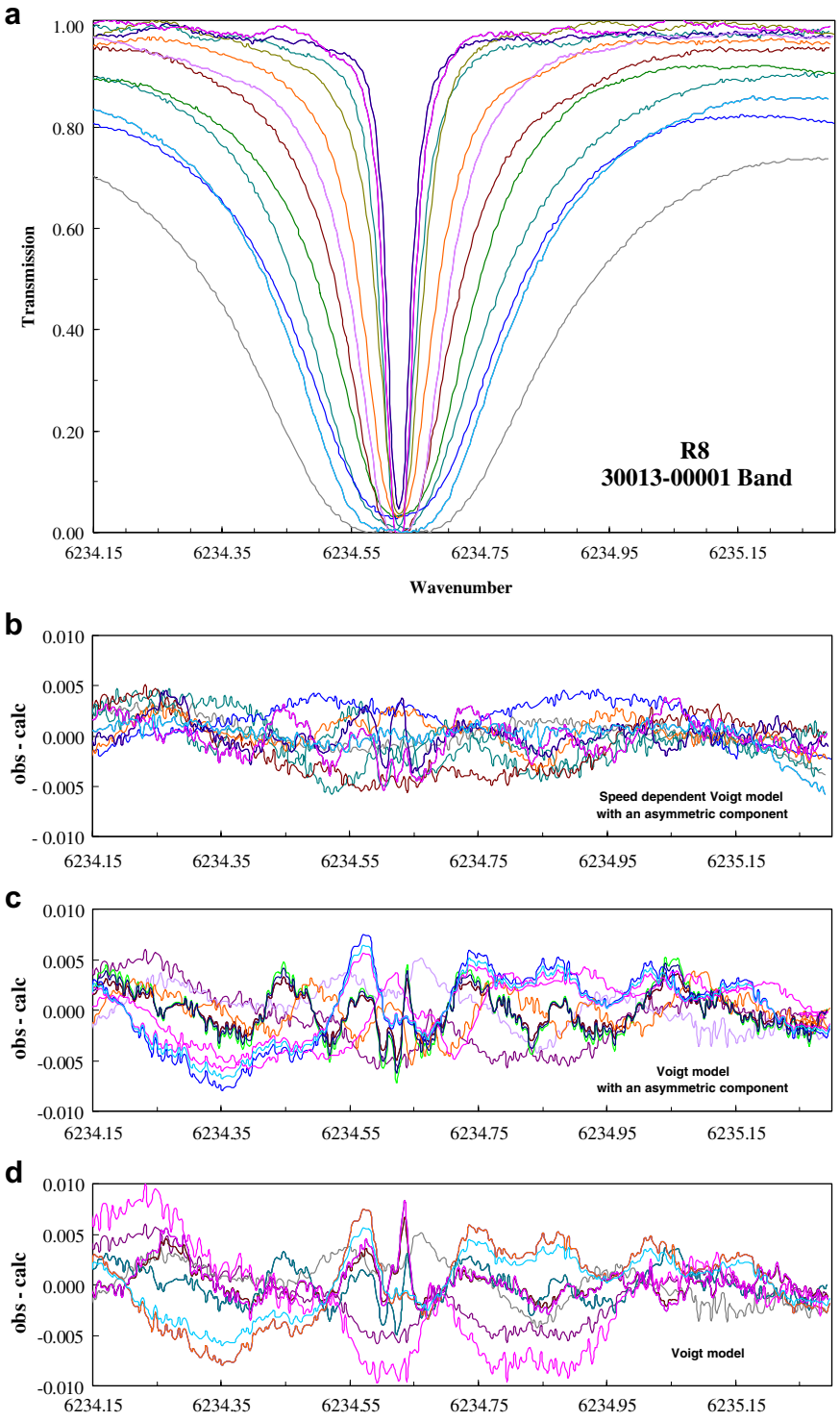

Fig. 2. Sample of the multi-spectrum fit in the spectral region of R(8) of the 30013 ← 00001 band. (a) Overlaid high-purity carbon dioxide spectra used in the multi-spectrum fits. (b) Weighted fit residuals from a fit using the Speed Dependent Voigt profile with an asymmetric line mixing component. (c) Weighted fit residuals from a fit using the Voigt profile with an asymmetric line mixing component. (d) Weighted fit residuals from a fit using the Voigt profile.

ity e ↔ e. For small deviations from room temperature, the partition function can be approximated as [29]

$$Q_{\mathrm{R}}(T) = Q_{\mathrm{R}}(296)\frac{T}{296} \tag{10}$$

with $Q_{\mathrm{R}}(296) = 236.60$. For the case of $\Delta l = 0$ and $\Delta J = \pm 1$, L can be written as

$$L = \left(\frac{m^2 - l^2}{|m|}\right) \tag{11}$$

where $m = -J''$ for the P branch and $J'' + 1$ for the R branch where $''$ denotes the lower rotational energy level and $'$ denotes the upper one. The Herman–Wallis factor is given by

$$F = (1 + a_1 m + a_2 m^2 + a_3 m^3)^2 F' \tag{12}$$

for the case of P and R branches $F' = 1$ when $\Delta l = 0$.

The measured strengths were converted to those at 296 K using Eqs. (8) and (10). We define a parameter β as

$$\beta' = \frac{S \exp\left(\frac{-hcE''}{kT}\right)}{g\left[1 - \exp\left(\frac{-hcv}{kT}\right)\right]} \frac{v_0}{v} \frac{Q_R}{L} \tag{13}$$

and from Eq. (8)

$$\beta' = S_{sb} F \tag{14}$$

Measured strengths were fitted to Eqs. (13) and (14). S_{sb} and F were determined through a least-square fit for β' using a program written in Matlab.

All line parameters retrieved from our spectra were converted to 296 K and to the natural abundance of CO_2 to facilitate comparison with other studies. Table 2 lists the calculated vibrational band strength S_v and the Herman–Wallis constants (F-factor) of CO_2 at 296 K in the $30013 \leftarrow 00001$ and $30012 \leftarrow 00001$ bands. Table 2 also lists the maximum J values for each study. Values of the same parameters available in the literature are also listed, but we are not confident that all values are reported at natural abundance and 296 K. The last column denotes the other studies.

In Table 3, we report the measured line intensities along with the values calculated with the parameters reported for our study in Table 2. The percentage difference between our calculated and observed intensities is also included. We compare our intensities with similar values available in the literature in Figs. 3 and 4. The results are plotted against m where $m = -J$ for P-branch transitions and $m = J + 1$ for R-branch transitions. It can be seen that the intensities from our present study agree best with the recent studies [29,31,32]. There is also a worrisome systematic difference between all the measured intensities and those from the HITRAN 2004 database.

3.2. Self-broadened widths and shift coefficients

The half width coefficients were fitted assuming a linear pressure dependence using the relation

$$\gamma^0 = \frac{\gamma}{p} \tag{15}$$

where, γ^0 is the retrieved broadening coefficient, γ is the measured broadened half width of the spectral line and p is the total sample pressure. The retrieved values for each spectral line were converted to those corresponding to 296 K using the equation

$$\gamma^0(296\ \mathrm{K}) = \gamma^0(T)\left[\frac{T}{296}\right]^n \tag{16}$$

where n is the temperature dependent coefficient. The value of n was assumed to be 0.75 following the assumption of Suarez and Valero [39]. Self-induced pressure shift were modeled using the expression

$$\delta^0 = \frac{v - v_0}{p} \tag{17}$$

Table 2a
Band strength parameters of CO_2 at 296 K in the $30013 \leftarrow 00001$ band

Band center (cm^{-1})	Band strength $\times 10^{22}$ (cm^{-1}/(molecule cm^{-2}))	$a_1 \times 10^4$	$a_2 \times 10^5$	J'_{max}	Reference
6227.9166	4.420(4)	2.782(88)	1.826(26)	67	[29]
6227.9166	4.466(6)	2.768(140)	1.897(46)	59	[28]
6227.9166	4.478(56)	−1.746(1101)	3.699(373)	59	[15]
6227.9166	4.387(31)	0.950(1918)		29	[25]
6227.9166	4.486(4)	2.864(109)	1.761(42)	51	[27]
6227.9166	4.515	8.9950	4.185	75	[21]
6227.9166	4.4133(5)	2.880(11)	1.711(4)	74	[32]
6227.9166	4.4276(8)	2.889(20)	1.717(10)	56	Our study

Table 2b
Band strength parameters of CO_2 at 296 K in the $30012 \leftarrow 00001$ band

Band center (cm^{-1})	Band strength $\times 10^{22}$ (cm^{-1}/(molecule cm^{-2}))	$a_1 \times 10^4$	$a_2 \times 10^5$	$a_3 \times 10^7$	J'_{max}	Reference
6347.8510	4.519(4)	2.648(90)	−1.510(26)		69	[29]
6347.8510	4.544(8)	2.251(176)	−1.402(59)		57	[28]
6347.8510	4.568(74)	−4.831(1541)	1.964(519)		57	[15]
6347.8510	4.495(48)	7.207(3334)	−3.740(653)		67	[18]
6347.8510	4.567(3)	2.388(80)	−1.502(31)		51	[27]
6347.8510	4.437	9.080	−0.240	−7.76	73	[21]
6347.8510	4.5138(6)	2.762(11)	−1.6032(44)		74	[31]
6347.8510	4.4977(4)	2.752(22)	−1.5975(34)		56	Our study

Table 3
Measured and calculated line intensities in the 30013 ← 00001 and 30012 ← 00001 bands

m	30013 ← 00001 band				30012 ← 00001 band			
	Position (cm^{-1})	Measured intensity (cm^{-1}/molecule × cm^{-2})	Calculated intensity (cm^{-1}/molecule × cm^{-2})	% Diff.	Position (cm^{-1})	Measured intensity (cm^{-1}/molecule × cm^{-2})	Calculated intensity (cm^{-1}/molecule × cm^{-2})	% Diff.
−56	6173.1694	2.31E−25	2.38E−25	3.1	6292.9968	2.03E−25	1.96E−25	−3.3
−54	6175.5288	3.46E−25	3.47E−25	0.4	6295.3198	2.91E−25	2.90E−25	−0.3
−52	6177.8566	4.83E−25	4.98E−25	3.2	6297.6187	4.33E−25	4.23E−25	−2.3
−50	6180.153	7.00E−25	7.04E−25	0.6	6299.8931	6.03E−25	6.06E−25	0.5
−48	6182.4182	9.85E−25	9.78E−25	−0.7	6302.1427	8.55E−25	8.52E−25	−0.3
−46	6184.6526	1.36E−24	1.34E−24	−1.7	6304.3668	1.19E−24	1.18E−24	−0.5
−44	6186.8561	1.79E−24	1.80E−24	0.2	6306.5652	1.58E−24	1.60E−24	1.5
−42	6189.0292	2.38E−24	2.37E−24	−0.3	6308.7376	2.11E−24	2.14E−24	1.4
−40	6191.1719	3.05E−24	3.08E−24	1.0	6310.8834	2.83E−24	2.82E−24	−0.6
−38	6193.2845	3.96E−24	3.94E−24	−0.6	6313.0025	3.64E−24	3.63E−24	−0.3
−36	6195.3672	4.94E−24	4.94E−24	0.0	6315.0944	4.65E−24	4.60E−24	−1.1
−34	6197.4202	6.11E−24	6.08E−24	−0.5	6317.1589	5.74E−24	5.72E−24	−0.3
−32	6199.4437	7.40E−24	7.35E−24	−0.6	6319.1957	7.06E−24	6.98E−24	−1.1
−30	6201.4378	8.57E−24	8.73E−24	1.8	6321.2045	8.46E−24	8.36E−24	−1.2
−28	6203.4027	1.02E−23	1.02E−23	−0.2	6323.1852	9.90E−24	9.80E−24	−0.9
−26	6205.3387	1.16E−23	1.16E−23	−0.4	6325.1374	1.13E−23	1.13E−23	0.1
−24	6207.2457	1.28E−23	1.30E−23	0.9	6327.0609	1.27E−23	1.27E−23	0.0
−22	6209.124	1.43E−23	1.42E−23	−0.6	6328.9556	1.40E−23	1.40E−23	−0.6
−20	6210.9737	1.49E−23	1.51E−23	2.0	6330.8212	1.51E−23	1.50E−23	−1.0
−18	6212.7949	1.60E−23	1.58E−23	−1.1	6332.6577	1.58E−23	1.57E−23	−0.7
−16	6214.5877	1.59E−23	1.60E−23	0.9	6334.4648	1.61E−23	1.60E−23	−0.8
−14	6216.3522	1.59E−23	1.57E−23	−0.7	6336.2424	1.57E−23	1.58E−23	0.5
−12	6218.0886	1.50E−23	1.49E−23	−0.5	6337.9904	1.50E−23	1.50E−23	0.1
−10	6219.7967	1.35E−23	1.36E−23	0.4	6339.7086	1.37E−23	1.37E−23	−0.2
−8	6221.4768	1.17E−23	1.17E−23	−0.2	6341.397	1.19E−23	1.18E−23	−0.3
−6	6223.1288	9.20E−24	9.28E−24	0.9	6343.0555	9.41E−24	9.40E−24	−0.1
−4	6224.7527	6.41E−24	6.45E−24	0.7	6344.684	6.58E−24	6.55E−24	−0.5
−2	6226.3487	3.34E−24	3.32E−24	−0.7	6346.2825	3.39E−24	3.37E−24	−0.7
1	6228.69	1.73E−24	1.68E−24	−2.8	6348.6238	1.68E−24	1.71E−24	1.3
3	6230.2158	4.98E−24	4.99E−24	0.4	6350.147	5.00E−24	5.07E−24	1.4
5	6231.7134	8.03E−24	8.12E−24	1.2	6351.6402	8.07E−24	8.23E−24	2.0
7	6233.1829	1.09E−23	1.09E−23	0.5	6353.1031	1.11E−23	1.11E−23	−0.1
9	6234.6241	1.32E−23	1.33E−23	0.7	6354.536	1.33E−23	1.34E−23	0.8
11	6236.037	1.52E−23	1.52E−23	−0.2	6355.9388	1.52E−23	1.53E−23	0.4
13	6237.4214	1.67E−23	1.65E−23	−1.0	6357.3116	1.64E−23	1.66E−23	0.8
15	6238.7773	1.70E−23	1.72E−23	1.3	6358.6544	1.71E−23	1.72E−23	0.6
17	6240.1045	1.75E−23	1.74E−23	−0.5	6359.9673	1.75E−23	1.74E−23	−0.8
19	6241.4028	1.71E−23	1.71E−23	0.2	6361.2504	1.72E−23	1.70E−23	−1.5
21	6242.6722	1.63E−23	1.64E−23	0.3	6362.5038	1.65E−23	1.62E−23	−1.9
23	6243.9124	1.53E−23	1.53E−23	0.3	6363.7276	1.50E−23	1.50E−23	0.0
25	6245.1233	1.39E−23	1.40E−23	1.0	6364.922	1.38E−23	1.36E−23	−1.1
27	6246.3046	1.25E−23	1.25E−23	0.5	6366.087	1.22E−23	1.21E−23	−1.1
29	6247.4562	1.10E−23	1.10E−23	−0.2	6367.2229	1.05E−23	1.05E−23	0.1
31	6248.5779	9.41E−24	9.43E−24	0.2	6368.3299	9.09E−24	8.98E−24	−1.1
33	6249.6694	7.90E−24	7.95E−24	0.7	6369.4081	7.53E−24	7.51E−24	−0.3
35	6250.7306	6.59E−24	6.58E−24	−0.1	6370.4577	6.18E−24	6.16E−24	−0.4
37	6251.7611	5.37E−24	5.35E−24	−0.5	6371.479	4.98E−24	4.96E−24	−0.3
39	6252.7607	4.23E−24	4.27E−24	0.9	6372.4722	3.90E−24	3.82E−24	−1.9
41	6253.7292	3.36E−24	3.35E−24	−0.3	6373.4376	3.00E−24	2.97E−24	−0.8
43	6254.6664	2.62E−24	2.58E−24	−1.5	6374.3755	2.29E−24	2.27E−24	−0.8
45	6255.5719	1.92E−24	1.96E−24	1.9	6375.2861	1.69E−24	1.70E−24	0.6
47	6256.4455	1.47E−24	1.46E−24	−0.4	6376.1699	1.22E−24	1.25E−24	3.0
49	6257.2869	1.08E−24	1.07E−24	−0.6	6377.0271	8.82E−25	9.09E−25	3.0
51	6258.096	7.76E−25	7.72E−25	−0.6	6377.8581	6.26E−25	6.47E−25	3.4
53	6258.8723	5.63E−25	5.47E−25	−2.8	6378.6632	4.40E−25	4.53E−25	3.0
55	6259.6157	3.85E−25	3.82E−25	−0.7	6379.443	3.21E−25	3.12E−25	−2.7
56	6260.3258	2.56E−25	2.62E−25	2.6				

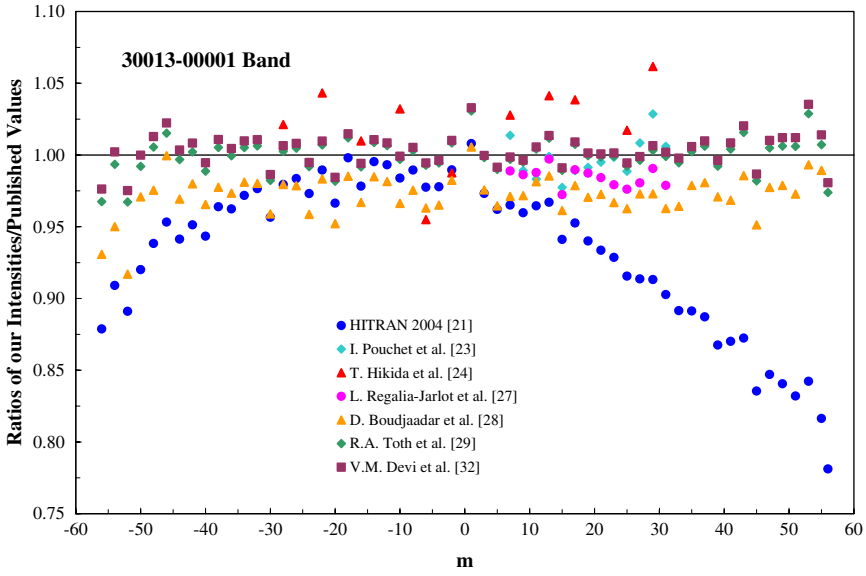

Fig. 3. Comparisons between our line intensities for transitions in the 30013 ← 00001 band and published results. The intensity ratios are plotted against m where $m = -J$ for P-branch transitions and $m = J + 1$ for R-branch transitions.

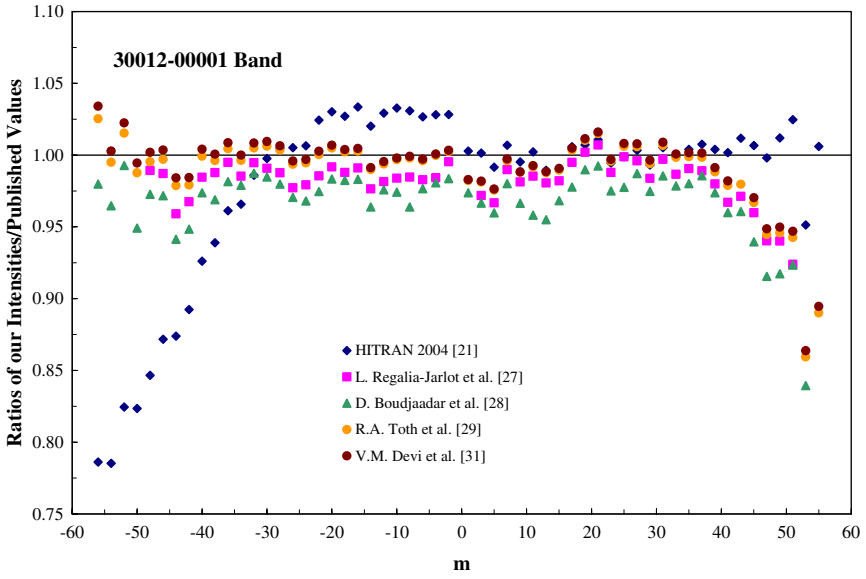

Fig. 4. Ratios of our line intensities for transitions in the 30012 ← 00001 band and published results plotted against m.

where δ^0 is the pressure induced shift, v is the measured line position, v_0 is the position at zero pressure, and p is the total pressure of the sample.

Pressure induced self-broadening and shifts were measured for 56 transitions from P(56) to R(54) using both Voigt and Speed Dependent Voigt profiles. The retrieved broadening parameters are plotted against m values in Fig. 5. All other measurements agree within 5% for the same J values in P and R branches. Our measurements are in good agreement with previous studies. The error bars for the results from Ref. [15] are not included since the parameter error is very high compared to other studies presented cluttering the diagram. The graph does not show the values obtained from the Exponential Power Gap (EPG) calculation—they are discussed in Section 4.

The measured self-pressure induced shifts are plotted in Fig. 6, where measurements available in the literature are overlaid. Results from De Rosa et al. [30] are not plotted, since the values deviate greatly from our results. Parameter errors are less than 4% for the values fitted with the Speed Dependent Voigt profile. The shifts retrieved with the Voigt profile have a parameter error below 5% except for the R(0) line for which it is 7%. The retrieved values are close to the results from Refs. [30–32]. The results reported in Ref. [18] have a parameter error of 5% which is not shown in the plot. The scatter in our broadening results occurs at

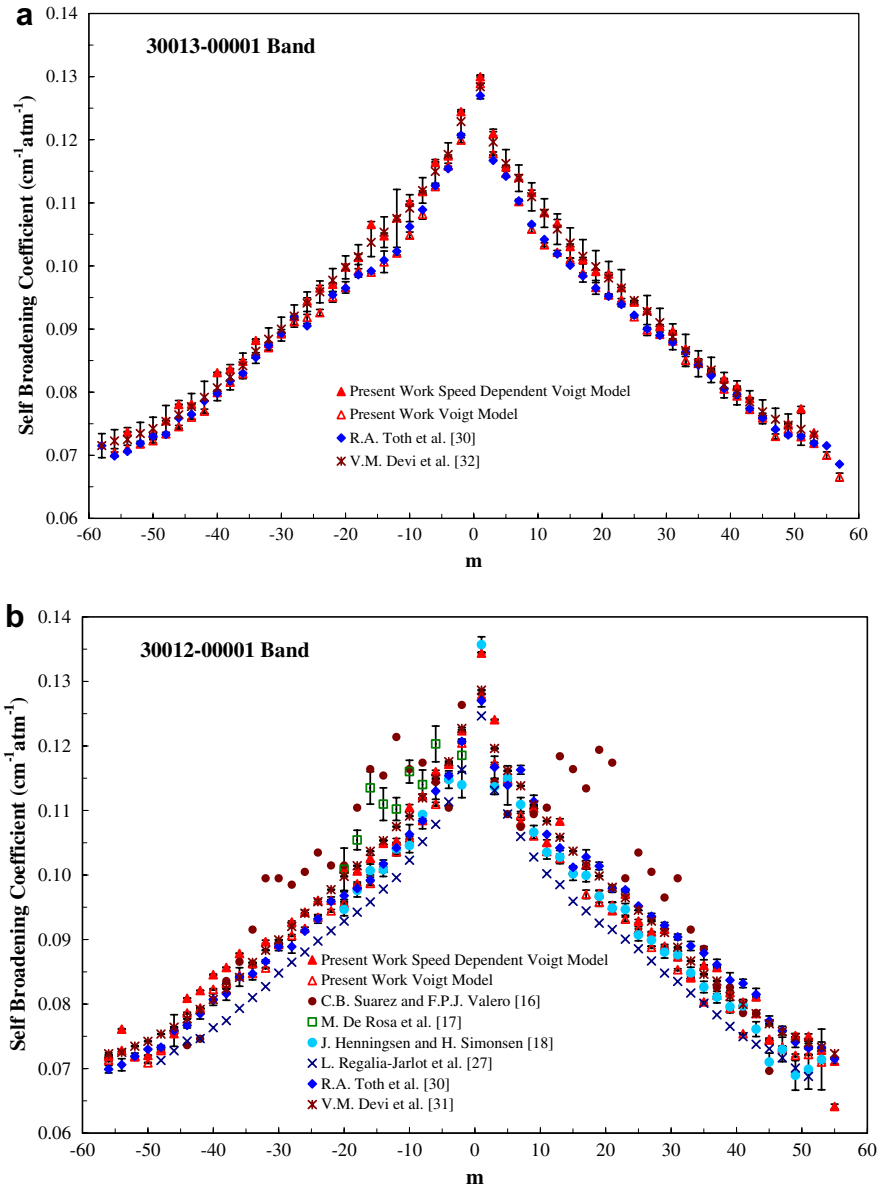

Fig. 5. Comparison of measured self-broadening coefficients for the transitions in the (a) 30013 ← 00001 band and (b) 30012 ← 00001 band, and published results. All measurements are plotted as a function of the *m* value.

high *J* values or in spectral regions where the transitions studied here overlap with hot band transitions.

3.3. Weak line mixing coefficients

CO_2 is the gas of choice for satellite remote sensing of atmospheric temperature profiles. The temperature retrievals from satellite remote sensing data rely on having available a correct model of the absorption profile. If a number of apparently small effects like line mixing, pressure shifts, Dicke narrowing, and speed dependence are neglected errors of up to several percent for the absorption coefficient may occur. Such errors cannot be tolerated as they become more and more significant as the accuracy and precision of space instrumentation improves. For example, current measurement requirements for atmospheric temperature are of the order of 1 K which in turn requires an understanding of the spectroscopy at the level better than 1% [40]. At this level of accuracy, many of the effects mentioned above become significant.

Closely spaced spectral lines at high pressures are broadened and overlap considerably to the extent that they cannot be considered isolated. Inelastic collisions transfer the molecular population between neighboring energy levels and a line mixing (or "line coupling") process occurs. Such inelastic coupling collisions are no longer effective in broadening the spectral lines [41] and are causing a transfer of intensity from some parts of the spectrum to others. The impact approximation assumes that the collisions are binary and are of a negligible short duration compared with

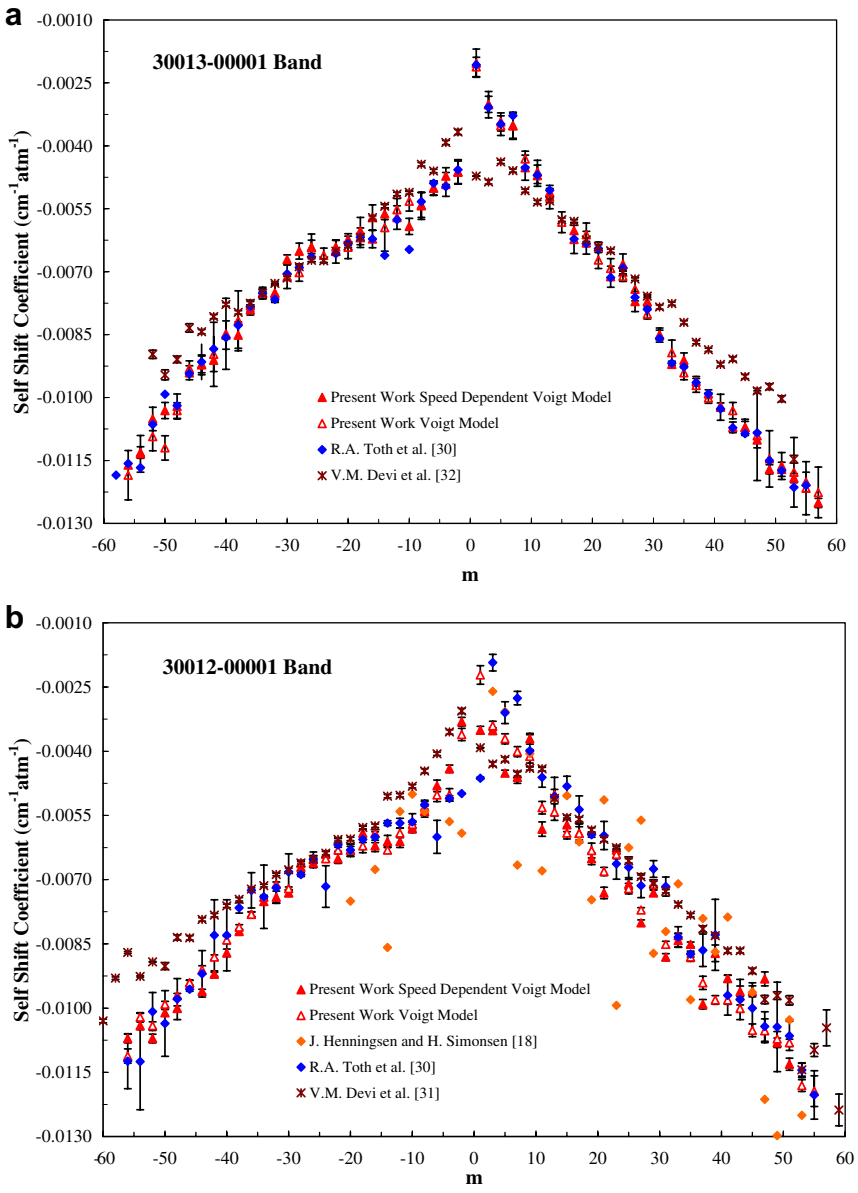

Fig. 6. Comparison of measured self-shift coefficients for the transitions in the (a) 30013 ← 00001 band and (b) 30012 ← 00001 band, and published results. All measurements are plotted as a function of the m value.

the time between collisions. Within the impact theory of the spectral shape, and within the Rozenkranz [42] approximation of weak overlapping, the collisional absorption coefficient $\alpha(v)$ can be written as the sum of a Lorentz with a mixing term for each line contributing to the spectrum as [43]

$$\alpha(v) = \frac{1}{\pi}\sum_i S_i \frac{pY_i^o(v - v_i) + p\gamma_i^o}{(v - v_i)^2 + (p\gamma_i^o)^2} \tag{18}$$

where p is the total pressure, i represents the line with quantum numbers $v'J' \leftarrow v''J''$ where $''$ denotes the lower vibrational state and $'$ the upper one, v_i is the wavenumber of the line including the collisional shift δ_i ($\delta = v_i - v_0$ with v_0 being the unperturbed wavenumber), γ_i^o is its half width, and Y_i^o is its line mixing parameter related to the off-diagonal element of the relaxation matrix. For other line profiles (Voigt, Speed Dependent Voigt, Galatry, etc.) the line mixing effect is computed by adding the corresponding dispersive profile multiplied by the pY_i^o factor, to the (standard) non-dispersive profile.

The non-linear least-square fit was performed for the expression

$$\tau(v) = \int_{-\infty}^{+\infty} \mathrm{ILS}(v - v')[\exp(-lP\alpha(v'))]\,\mathrm{d}v' \tag{19}$$

where $\tau(v)$ is the transmission coefficient, ILS is the instrumental line shape function, l is the pathlength, P the species partial pressure and α is the absorption coefficient including the corresponding line shape model (Voigt or Speed Dependent Voigt). The instrumental line shape was

assumed to be a modified *sinc* function, as described at the beginning of Section 3. The first order line mixing coefficient Y_0 for each spectral line were calculated with the equation

Table 4a
Spectral line parameters for the 30013 ← 00001 band

m	Position (cm^{-1})	Intensity (cm^{-1}/molecule cm^{-2})	γ^0 (cm^{-1} atm^{-1})		δ^0 (cm^{-1} atm^{-1})		Y_0 (atm^{-1})
			VOIGT	SDV	VOIGT	SDV	SDV
−56	6173.169436	2.308(36) E−25	0.0704(6)	0.0725(1)	−0.0118(5)	−0.0116(1)	
−54	6175.528804	3.458(34) E−25	0.0711(5)	0.0734(1)	−0.0113(4)	−0.0113(1)	0.0064(5)
−52	6177.856588	4.832(27) E−25	0.0718(4)	0.0731(1)	−0.0109(3)	−0.0105(1)	0.0051(4)
−50	6180.152998	6.999(23) E−25	0.0723(3)	0.0734(1)	−0.0110(2)	−0.0103(1)	0.0056(4)
−48	6182.418249	9.852(60) E−25	0.0734(2)	0.0753(2)	−0.0103(1)	−0.0102(1)	0.0052(4)
−46	6184.652553	1.359(3) E−24	0.0745(2)	0.0776(1)	−0.0093(1)	−0.0094(1)	0.0051(4)
−44	6186.856124	1.793(2) E−24	0.0760(3)	0.0778(1)	−0.0092(2)	−0.0092(1)	0.0053(3)
−42	6189.029173	2.381(12) E−24	0.0770(3)	0.0794(1)	−0.0089(7)	−0.0091(1)	0.0048(3)
−40	6191.171908	3.051(11) E−24	0.0799(3)	0.0814(2)	−0.0084(8)	−0.0085(1)	0.0054(3)
−38	6193.284533	3.958(8) E−24	0.0816(3)	0.0833(1)	−0.0081(7)	−0.0085(1)	0.0036(5)
−36	6195.367248	4.935(33) E−24	0.0829(2)	0.0845(1)	−0.0078(1)	−0.0079(1)	0.0047(5)
−34	6197.420244	6.112(35) E−24	0.0860(2)	0.0868(3)	−0.0075(1)	−0.0075(2)	0.0039(4)
−32	6199.443709	7.400(31) E−24	0.0871(3)	0.0876(1)	−0.0075(1)	−0.0075(1)	0.0039(4)
−30	6201.437820	8.573(26) E−24	0.0894(5)	0.0896(3)	−0.0071(2)	−0.0067(1)	0.0038(4)
−28	6203.402748	1.018(6) E−23	0.0912(4)	0.0919(3)	−0.0070(2)	−0.0065(1)	0.0048(4)
−26	6205.338653	1.164(5) E−23	0.0918(9)	0.0940(2)	−0.0064(3)	−0.0064(1)	0.0043(5)
−24	6207.245685	1.284(5) E−23	0.0926(5)	0.0961(3)	−0.0066(1)	−0.0065(1)	0.0037(5)
−22	6209.123984	1.425(9) E−23	0.0951(8)	0.0971(3)	−0.0065(2)	−0.0064(1)	0.0031(3)
−20	6210.973679	1.485(4) E−23	0.0966(9)	0.0994(4)	−0.0064(2)	−0.0062(3)	0.0027(1)
−18	6212.794885	1.595(9) E−23	0.0992(9)	0.1009(7)	−0.0061(9)	−0.0060(3)	0.0009(1)
−16	6214.587708	1.585(8) E−23	0.0990(1)	0.1031(3)	−0.0062(2)	−0.0057(1)	0.0016(1)
−14	6216.352238	1.585(6) E−23	0.1006(17)	0.1050(6)	−0.0059(5)	−0.0056(2)	−0.0003(1)
−12	6218.088553	1.501(7) E−23	0.1020(3)	0.1071(4)	−0.0055(2)	−0.0057(1)	−0.0011(1)
−10	6219.796718	1.352(8) E−23	0.1049(5)	0.1096(5)	−0.0053(2)	−0.0059(2)	−0.0043(5)
−8	6221.476784	1.170(5) E−23	0.1082(7)	0.1114(3)	−0.0054(3)	−0.0054(1)	−0.0071(6)
−6	6223.128787	9.197(56) E−24	0.1126(3)	0.1151(3)	−0.0050(1)	−0.0050(1)	−0.0098(6)
−4	6224.752748	6.408(53) E−24	0.1158(4)	0.1169(3)	−0.0049(2)	−0.0047(2)	−0.0158(14)
−2	6226.348676	3.339(9) E−24	0.1199(3)	0.1239(3)	−0.0046(2)	−0.0046(3)	−0.0237(21)
1	6228.689985	1.729(6) E−24	0.1289(1)	0.1294(4)	−0.0021(2)	−0.0020(3)	0.0305(18)
3	6230.215765	4.976(14) E−24	0.1178(2)	0.1204(2)	−0.0030(1)	−0.0030(2)	0.0236(14)
5	6231.713422	8.025(39) E−24	0.1146(3)	0.1155(4)	−0.0035(2)	−0.0034(3)	0.0171(23)
7	6233.182896	1.087(7) E−23	0.1102(3)	0.1135(4)	−0.0035(2)	−0.0035(2)	0.0130(18)
9	6234.624116	1.321(5) E−23	0.1058(5)	0.1112(5)	−0.0043(1)	−0.0045(2)	0.0078(8)
11	6236.036992	1.521(1) E−23	0.1033(3)	0.1080(2)	−0.0046(2)	−0.0047(1)	0.0063(3)
13	6237.421424	1.665(3) E−23	0.1022(3)	0.1063(2)	−0.0052(2)	−0.0051(1)	0.0032(2)
15	6238.777296	1.701(6) E−23	0.1010(2)	0.1031(4)	−0.0058(2)	−0.0057(1)	0.0016(1)
17	6240.104478	1.751(8) E−23	0.0989(14)	0.1018(7)	−0.0062(3)	−0.0060(2)	0.0002(1)
19	6241.402828	1.708(10) E−23	0.0966(10)	0.0995(3)	−0.0061(2)	−0.0063(1)	−0.0010(1)
21	6242.672191	1.633(8) E−23	0.0954(1)	0.0983(6)	−0.0067(2)	−0.0064(2)	−0.0023(3)
23	6243.912398	1.527(6) E−23	0.0946(2)	0.0962(5)	−0.0069(2)	−0.0071(2)	−0.0033(3)
25	6245.123271	1.386(10) E−23	0.0919(1)	0.0949(5)	−0.0071(1)	−0.0068(2)	−0.0045(5)
27	6246.304618	1.245(3) E−23	0.0898(8)	0.0926(2)	−0.0074(2)	−0.0077(1)	−0.0054(4)
29	6247.456239	1.099(5) E−23	0.0892(3)	0.0903(3)	−0.0080(1)	−0.0077(1)	−0.0061(6)
31	6248.577920	9.406(10) E−24	0.0881(3)	0.0893(1)	−0.0085(1)	−0.0085(1)	−0.0068(5)
33	6249.669442	7.896(67) E−24	0.0850(6)	0.0865(2)	−0.0089(3)	−0.0092(1)	−0.0070(10)
35	6250.730575	6.587(11) E−24	0.0850(3)	0.0842(1)	−0.0094(1)	−0.0091(1)	−0.0075(7)
37	6251.761081	5.374(37) E−24	0.0834(2)	0.0840(1)	−0.0097(1)	−0.0096(1)	−0.0090(6)
39	6252.760717	4.232(6) E−24	0.0805(1)	0.0817(1)	−0.0100(1)	−0.0099(1)	−0.0090(6)
41	6253.729232	3.360(6) E−24	0.0794(4)	0.0805(1)	−0.0102(3)	−0.0102(1)	−0.0090(9)
43	6254.666372	2.621(6) E−24	0.0773(1)	0.0786(1)	−0.0103(1)	−0.0107(1)	−0.0102(12)
45	6255.571877	1.921(6) E−24	0.0759(1)	0.0761(2)	−0.0107(1)	−0.0107(1)	−0.0099(10)
47	6256.445485	1.466(14) E−24	0.0730(3)	0.0754(1)	−0.0109(10)	−0.0110(1)	−0.0109(9)
49	6257.286932	1.076(7) E−24	0.0741(8)	0.0747(1)	−0.0114(6)	−0.0117(1)	−0.0115(9)
51	6258.095953	7.762(60) E−25	0.0729(3)	0.0738(1)	−0.0116(3)	−0.0117(1)	−0.0110(8)
53	6258.872284	5.631(27) E−25	0.0719(3)	0.0733(1)	−0.0117(8)	−0.0119(2)	−0.0120(12)
55	6259.615664	3.848(34) E−25	0.0700(5)	0.0723(1)	−0.0121(6)	−0.0120(1)	
56	6260.325831	2.555(38) E−25	0.0665(6)	0.0721(2)	−0.0122(6)	−0.0125(1)	

$$Y_0 = \frac{Y_i}{P} \tag{20}$$

where Y_i is the measured line mixing coefficient and P is the total pressure of the sample.

All the measured line parameters are listed in Tables 4a and 4b along with the experimental uncertainties. The first column lists the m values, and the next two columns list the positions and intensities, respectively. Positions are in units

Table 4b
Spectral line parameters for the 30012 ← 00001 band

m	Position (cm^{-1})	Intensity (cm^{-1}/(molecule cm^{-2}))	γ^0 (cm^{-1} atm^{-1})		δ^0 (cm^{-1} atm^{-1})		Y_0 (atm^{-1})
			VOIGT	SDV	VOIGT	SDV	SDV
−56	6292.996793	2.028(201) E−25	0.0713(2)	0.0719(1)	−0.0111(2)	−0.0107(1)	0.0057(7)
−54	6295.319763	2.913(48) E−25	0.0728(1)	0.0761(1)	−0.0102(1)	−0.0104(1)	0.0059(6)
−52	6297.618698	4.328(21) E−25	0.0718(1)	0.0719(1)	−0.0104(1)	−0.0107(1)	0.0057(7)
−50	6299.893141	6.027(54) E−25	0.0709(1)	0.0721(1)	−0.0099(1)	−0.0101(1)	0.0051(4)
−48	6302.142653	8.550(30) E−25	0.0728(1)	0.0731(1)	−0.0097(1)	−0.0100(1)	0.0052(8)
−46	6304.366820	1.185(5) E−24	0.0761(1)	0.0754(1)	−0.0094(1)	−0.0094(1)	0.0071(9)
−44	6306.565247	1.581(6) E−24	0.0786(1)	0.0809(1)	−0.0091(1)	−0.0096(1)	0.0077(3)
−42	6308.737560	2.114(9) E−24	0.0794(1)	0.0821(1)	−0.0088(1)	−0.0092(1)	0.0073(3)
−40	6310.883410	2.833(7) E−24	0.0823(1)	0.0846(1)	−0.0084(1)	−0.0087(1)	0.0046(7)
−38	6313.002450	3.643(17) E−24	0.0832(1)	0.0857(1)	−0.0081(1)	−0.0082(1)	0.0067(4)
−36	6315.094370	4.652(40) E−24	0.0844(1)	0.0878(1)	−0.0078(1)	−0.0078(1)	0.0059(3)
−34	6317.158870	5.736(58) E−24	0.0847(1)	0.0863(1)	−0.0074(1)	−0.0075(1)	0.0079(3)
−32	6319.195680	7.059(60) E−24	0.0856(1)	0.0897(2)	−0.0071(1)	−0.0074(1)	0.0065(6)
−30	6321.204520	8.459(368) E−24	0.0892(1)	0.0894(2)	−0.0072(1)	−0.0073(1)	0.0046(3)
−28	6323.185160	9.896(60) E−24	0.0906(1)	0.0927(2)	−0.0066(1)	−0.0067(1)	0.0046(3)
−26	6325.137350	1.125(8) E−23	0.0917(2)	0.0943(2)	−0.0065(1)	−0.0066(1)	0.0048(4)
−24	6327.060900	1.268(11) E−23	0.0935(2)	0.0961(2)	−0.0065(1)	−0.0064(1)	0.0035(3)
−22	6328.955590	1.403(4) E−23	0.0945(2)	0.0961(5)	−0.0063(1)	−0.0065(1)	0.0034(3)
−20	6330.821240	1.514(4) E−23	0.0956(3)	0.1009(4)	−0.0063(1)	−0.0063(1)	0.0028(4)
−18	6332.657690	1.581(6) E−23	0.0986(3)	0.1006(3)	−0.0062(1)	−0.0059(1)	0.0025(3)
−16	6334.464790	1.612(4) E−23	0.0987(3)	0.1026(4)	−0.0059(1)	−0.0062(1)	0.0012(3)
−14	6336.242380	1.571(10) E−23	0.1011(3)	0.1049(5)	−0.0063(1)	−0.0061(1)	−0.0005(4)
−12	6337.990360	1.502(7) E−23	0.1036(3)	0.1052(4)	−0.0059(1)	−0.0061(1)	−0.0019(4)
−10	6339.708600	1.373(6) E−23	0.1057(3)	0.1105(4)	−0.0057(1)	−0.0058(1)	−0.0041(3)
−8	6341.397010	1.185(5) E−23	0.1084(3)	0.1122(3)	−0.0053(1)	−0.0054(1)	−0.0076(4)
−6	6343.055515	9.414(4) E−24	0.1110(3)	0.1160(2)	−0.0050(2)	−0.0048(1)	−0.0117(5)
−4	6344.684033	6.580(30) E−24	0.1151(2)	0.1172(1)	−0.0050(2)	−0.0044(1)	−0.0152(1)
−2	6346.282512	3.393(22) E−24	0.1205(3)	0.1224(1)	−0.0036(1)	−0.0033(1)	−0.0366(12)
1	6348.623821	1.684(7) E−24	0.1278(3)	0.1344(1)	−0.0022(2)	−0.0035(1)	0.0735(1)
3	6350.147049	4.997(17) E−24	0.1173(2)	0.1144(2)	−0.0034(1)	−0.0035(2)	0.0285(8)
5	6351.640150	8.071(39) E−24	0.1147(2)	0.1148(1)	−0.0037(1)	−0.0045(1)	0.0224(5)
7	6353.103127	1.107(6) E−23	0.1092(3)	0.1082(3)	−0.0040(1)	−0.0046(1)	0.0139(5)
9	6354.535999	1.333(6) E−23	0.1061(4)	0.1104(3)	−0.0041(2)	−0.0037(1)	0.0077(4)
11	6355.938798	1.523(37) E−23	0.1037(4)	0.1050(4)	−0.0053(2)	−0.0058(2)	0.0052(5)
13	6357.311571	1.642(5) E−23	0.1026(6)	0.1084(4)	−0.0054(2)	−0.0050(1)	0.0039(4)
15	6358.654375	1.713(8) E−23	0.1007(6)	0.1008(4)	−0.0059(1)	−0.0057(2)	0.0024(10)
17	6359.967287	1.750(11) E−23	0.0970(7)	0.1016(6)	−0.0059(2)	−0.0059(2)	0.0004(13)
19	6361.250392	1.722(4) E−23	0.0958(6)	0.0972(4)	−0.0063(2)	−0.0065(1)	−0.0036(6)
21	6362.503794	1.647(4) E−23	0.0953(4)	0.0945(4)	−0.0068(1)	−0.0073(1)	−0.0027(5)
23	6363.727610	1.501(6) E−23	0.0932(3)	0.0971(3)	−0.0064(1)	−0.0063(1)	−0.0032(2)
25	6364.921972	1.378(4) E−23	0.0916(4)	0.0929(2)	−0.0072(1)	−0.0071(1)	−0.0036(4)
27	6366.087029	1.224(10) E−23	0.0888(2)	0.0912(1)	−0.0077(1)	−0.0080(1)	−0.0062(3)
29	6367.222942	1.052(7) E−23	0.0890(3)	0.0916(1)	−0.0071(1)	−0.0073(1)	−0.0072(3)
31	6368.329891	9.086(56) E−24	0.0853(1)	0.0873(2)	−0.0085(1)	−0.0088(1)	−0.0079(6)
33	6369.408072	7.534(46) E−24	0.0841(1)	0.0843(3)	−0.0083(1)	−0.0084(2)	−0.0091(16)
35	6370.457697	6.184(37) E−24	0.0803(2)	0.0860(1)	−0.0088(1)	−0.0085(1)	−0.0085(5)
37	6371.478995	4.977(31) E−24	0.0814(2)	0.0857(1)	−0.0094(1)	−0.0099(1)	−0.0097(8)
39	6372.472214	3.895(22) E−24	0.0794(2)	0.0818(2)	−0.0098(1)	−0.0087(2)	−0.0101(22)
41	6373.437620	2.995(16) E−24	0.0754(1)	0.0803(1)	−0.0098(1)	−0.0093(1)	−0.0083(14)
43	6374.375495	2.286(5) E−24	0.0785(1)	0.0811(1)	−0.0100(1)	−0.0096(1)	−0.0103(21)
45	6375.286144	1.691(17) E−24	0.0745(2)	0.0744(1)	−0.0105(2)	−0.0096(1)	−0.0097(26)
47	6376.169890	1.217(6) E−24	0.0731(3)	0.0733(1)	−0.0105(3)	−0.0093(2)	−0.0099(17)
49	6377.027075	8.824(35) E−25	0.0721(2)	0.0751(3)	−0.0107(2)	−0.0108(1)	
51	6377.858065	6.260(38) E−25	0.0722(1)	0.0750(3)	−0.0108(1)	−0.0113(1)	
53	6378.663244	4.40(42) E−25	0.0711(2)	0.0729(1)	−0.0118(1)		
55	6379.443023	3.21(46) E−25	0.0712(5)	0.0641(4)	−0.0119(4)		

of $cm^{-1}$and intensities are in cm^{-1}/(molecule cm^{-2}). The following columns show the half widths, self-induced pressure shifts and weak line mixing coefficient. Experimental uncertainties for the last digits of the parameters are given in parentheses.

4. Exponential power gap calculations for rotational transfer

Following the approach of Levy et al. [43] we use the relaxation matrix formalism to treat the CO_2 bands as a whole. The band's behavior over a range of pressures can be related to the elements of the relaxation matrix. Two approximations: the impact approximation and the approximation that the density matrix can be factored are made in this formalism. The impact approximation assumes that the collisions are binary and their duration is negligible compared with the time between consecutive collisions. The density matrix is factorized by dividing the gas sample into a large number of identical cells and considering one cell as the system while the remaining cells are referred to as thermal bath gas.

Line mixing coefficients can be quantified by the off-diagonal elements of the relaxation matrix along with the dipole transition moments [43] the diagonal elements of which represent the broadening and shift coefficients

$$W_{ii} = \alpha_{\mathrm{L}i} + \mathrm{i}\delta_i \tag{21}$$

where W_{ii} represents the diagonal elements, $\alpha_{\mathrm{L}i}$ are the Lorentz widths, and δ_i are the pressure-induced shifts.

The collisional transfer rates can be calculated using energy scaling laws. The fitting laws characterize the off-diagonal matrix elements of the relaxation matrix for any rotational state using a set of fitting parameters. We have calculated the relaxation matrix elements using an Exponential Power Gap (EPG) law [44–49] calculation for the rates of relaxation of the rotational states. The EPG law gives the collisional transfer rate κ_{jk}, from the lower rotational level k to a higher rotational level j as

$$\kappa_{jk} = a\left[\frac{|\Delta E_{jk}|}{B_0}\right]^{-b} \exp\left(\frac{-c|\Delta E_{jk}|}{B_0}\right) \tag{22}$$

where ΔE_{jk} is the energy gap between the two rotational states and B_0 is the rotational constant and a, b, and c are the parameters to be optimized. In thermodynamic equilibrium, the rates of population transfer is related through the detailed balance condition

$$\rho_k \kappa_{jk} = \rho_j \kappa_{kj} \tag{23}$$

where ρ_k is the population of the rotational level k. This relation fixes the rates of downward transitions relative to the upward transition rates.

Usually κ_{jk} is taken as the rates for the vibrational states with J even states. Since there exist only J even states for our band of interest and the B_0 values for the upper and lower vibrational states are nearly the same we assume the same collisional transfer rates for the rotational states in the upper and lower vibrational levels.

Population relaxation rates and the relaxation matrix elements can be related as described here. The width of a line or the diagonal elements of the relaxation matrix can be set to one half the sum of the total rates out of the lower and upper states involved in the transition

$$W_{kk} = \frac{1}{2}\left[\sum_j \kappa_{jk}\right]_{\text{upper}} + \frac{1}{2}\left[\sum_j \kappa_{jk}\right]_{\text{lower}} \tag{24}$$

where upper and lower denote the contribution from the upper and lower vibrational levels.

Off-diagonal elements of the relaxation matrix can be calculated (assuming the relaxation rates are related to them) as [44–48]

$$W_{jk} = -\beta\kappa_{jk} \tag{25}$$

where β is a constant.

The line mixing coefficient Y_{ok} for transitions between levels j and k can be expressed as a function of the off-diagonal matrix elements W_{jk} and the components of the dipole matrix element of the optical transition d_k

$$Y_{ok}(T) = 2\sum_{j\neq k} \frac{d_j}{d_k}\frac{W_{jk}}{\nu_k - \nu_j} \tag{26}$$

We used the values reported in Tables 4a and 4b for the broadening coefficients to determine the set of parameters a, b, c, and β, that best reproduce the broadening parameters with a fitting program written in Matlab. The non-linear fit used the Marquardt algorithm. The calculated values are $a = 6.101(2)\times 10^{-2}\,cm^{-1}\,atm^{-1}$, $b = 3.039(5)\times 10^{-2}$, and $c = 1.198(6)$ for the P-branch transitions in the $30012 \leftarrow 00001$ vibrational bands. For R-branch transitions: $a = 4.953(1)\times 10^{-2}$, $b = 2.583(5)\times 10^{-1}$, and $c = 1.252(7)$. The value used for β was 0.56. The results obtained for P-branch transitions in the $30013 \leftarrow 00001$ band are $a = 6.129(1)\times 10^{-2}$, $b = 3.053(5)\times 10^{-2}$, and $c = 1.190(5)$. The set of parameters that best fits R-branch broadening parameters is $a = 5.105(3)\times 10^{-2}$, $b = 2.721(6)\times 10^{-1}$, and $c = 1.223(6)$. The broadening and shift coefficients were calculated using these parameters, using the energy values from HITRAN 2004 [21]. The mixing coefficients were calculated using Eq. (26).

5. Energy Corrected Sudden calculations for rotational transfer

The Energy Corrected Sudden fitting law is a dynamically based expression in which the angular momentum transferred in molecular collisions is the main variable. In this approach the collisional rates involve a sum of products of angular momentum coupling coefficients and basis rate constants that depend on the angular momentum L, where L covers all rotational levels consistent with the symmetry of the active molecule.

In many instances the molecular collisions are not sudden and as a consequence the isolated lines are not Lorentzian in the wings. This deviation does not affect the width of the spectral line. The Energy Corrected

Sudden fitting law is an extension of the infinite-order sudden law (IOS) [49] to the case where molecular collisions are not sudden anymore [49–54]. Our study followed the implementation described in Ref. [52]. The relaxation matrix elements that connect two transitions ($J'_f \leftarrow J'_i$ and $J_f \leftarrow J_i$) of the $v_{1f}v_{2f}^{l_f}v_{3f} \leftarrow v_{1i}v_{2i}^{l_i}v_{3i}$ vibrational band at a given temperature T are

$$\begin{aligned}&\langle\langle J'_i l_i J'_f l_f | w(T) | J_i l_i J_f l_f \rangle\rangle \\ &= (2J'_i+1)\sqrt{(2J_f+1)(2J'_f+1)}(-1)^{l_i+l_f} \\ &\times \sum_{\text{Leven}\neq 0} \begin{pmatrix} J_i & L & J'_i \\ l_i & 0 & -l_i \end{pmatrix} \begin{pmatrix} J_f & L & J'_f \\ l_f & 0 & -l_f \end{pmatrix} \begin{pmatrix} J_i & J_f & 1 \\ j'_f & J_f & L \end{pmatrix} \\ &\times (2L+1)\frac{\Omega(J_i,T)}{\Omega(L,T)} Q(L,T) \end{aligned} \quad (27)$$

where (:::) and {:::} are $3J$ and $6J$ coefficients. Eq. (27) is used to calculate the "downward" transitions ($J'_i < J_i$) only, with the upward ones being obtained from detailed balance (Eq. (23)). The expression for the adiabaticity factor at a given temperature T was given in Ref. [54] as

$$\Omega(J,T) = \left\{1 + \frac{1}{24}\left[\frac{\omega_{J,J-2} d_c}{\bar{v}(T)}\right]^2\right\}^{-2} \quad (28)$$

where $\Delta E_{J,J-2}, \bar{v}, d_c$ are the wavenumber spacing between level J and $J-2$, the mean relative velocity in CO_2–CO_2 collisions, and the scaling length. The basic rates are expressed through an exponential power law dependence [51–53]

$$Q(J,T) = A(T)[L(L+1)]^{-\lambda(T)} \exp\left[-\beta(T)\frac{hcE_J}{k_B T}\right] \quad (29)$$

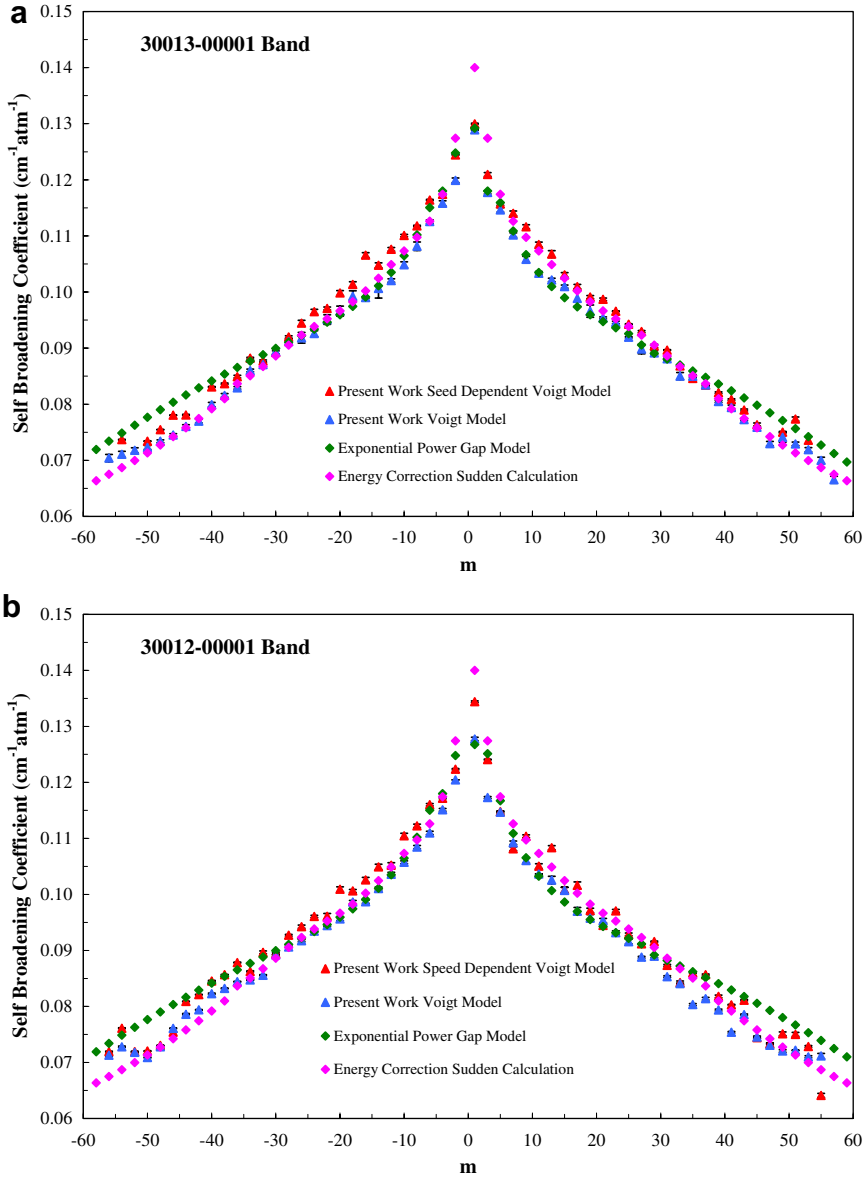

Fig. 7. Overlaid measured and calculated broadening parameters using the Exponential Power Gap law (EPG) plotted against m. The top panel presents results in the 30013 ← 00001 band. The bottom panel presents our results for the 30012 ← 00001 band.

where E_J is the rotational energy of level J. This type of scaling law is often referred to as the ECS–EP model that depends on the d_c, A, λ, and β parameters of the ECS–EP model. As in the case of the EPG calculations, all spectroscopic parameters needed to calculate the collisional rates are taken from the HITRAN 2004 database. Here we use only room temperature results as these are the only ones that are available. We find the room temperature parameters to be: $A = 0.0182\ \mathrm{cm}^{-1}/\mathrm{atm}$, $\lambda = 0.7396$, $\beta = 0.06$, and $d_c = 6.0$ Å, very close to the values reported in Ref. [52].

Once the off-diagonal elements of the relaxation matrix are calculated using the ECS implementation, the diagonal elements can be calculated using the expression [53]

$$W_{kk} = -\sum_{j \neq k} \frac{d_j}{d_k} W_{jk} \tag{30}$$

where d_k is the dipole matrix element of the optical transition k. The line mixing coefficients can be calculated using Eq. (26).

The software developed to perform Energy Corrected Sudden calculations was written in Matlab. The computations of Wigner $6J$ and $3J$ coefficients are not directly available in Matlab, so they must be obtained by third party sources. We originally used the Wigner coefficients "threej.m" and "sixj.m" obtained from MIT's Field Group Programming Library. The functions tended to break down at high J values, yielding infinities and undefined

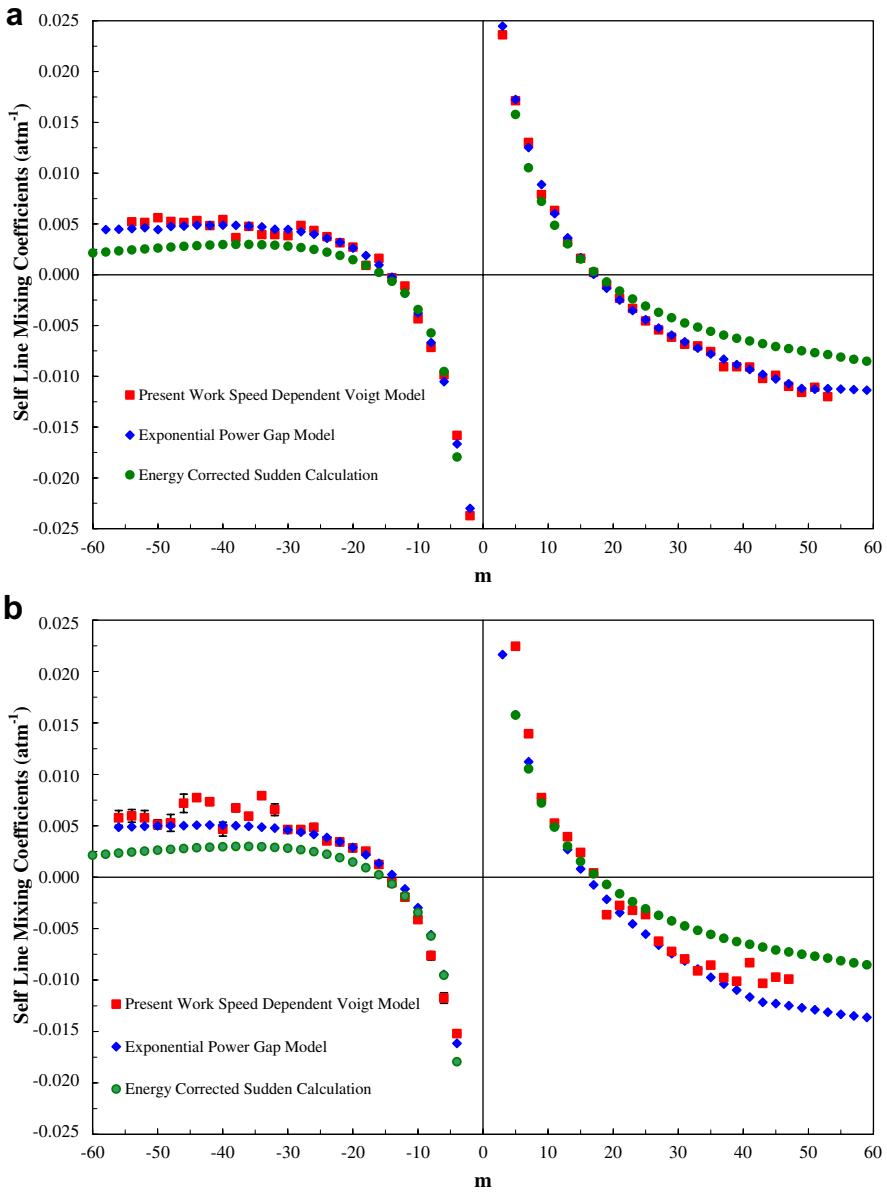

Fig. 8. Overlaid measured and calculated line mixing results parameters using the Exponential Power Gap law (EPG) and Energy Corrected Sudden (ECS) law, respectively. The top panel presents results in the 30013 ← 00001 band. The bottom panel presents our results for the 30012 ← 00001 band. All results are plotted against m.

values. This was due to the fact that the 3J and 6J symbol calculations extensively rely on sums of factorial calculations, and Matlab renders factorials greater than the 170th power as errors. We found that Mathematica's Wigner functions generate valid results for each relaxation matrix element. We were able to link Mathematica's kernel to Matlab using the Mathematica Symbolic Toolbox for MATLAB version 2.0 [55]. This package provides a dynamically linked library (DLL) that allows Mathematica functions to be called from Matlab.

Fig. 7 shows overlaid measured and calculated broadening parameters using the Exponential Power Gap law (EPG) plotted against m. Overlaid measured and calculated line mixing results parameters using the EPG law and Energy Corrected Sudden (ECS) law, respectively, are presented in Fig. 8. All results are plotted against m. In both figures the top panel presents results in the $30013 \leftarrow 00001$ band and the bottom panel presents our results for the $30012 \leftarrow 00001$ band. Both fitting laws used successfully modeled the entire range of rotational states. However, none of them fits perfectly the measured broadening parameters. For $|m|$ values between 10 and 35 both models provide a good agreement with the experimental results. The ECS model fails to reproduce well the measurements at very low $|m|$ values, whereas the EPG model seems to overestimate the broadening at $|m| > 37$. For the line mixing coefficients the EPG model seems to give an overall better agreement than the ECS model.

6. Conclusion

In this study, we have measured accurate values for self-broadening, self-shift coefficients using high-quality Fourier transform spectra. The results are in very good agreement with recent studies [29–32]. We observe a systematic difference between the broadening coefficients obtained using the Voigt profile and the ones obtained with the Speed Dependent Voigt profile. Overall, the Speed Dependent Voigt fitted broadening parameters are slightly higher than those obtained by a Voigt fit. This is expected because all calculated speed-dependent line profiles are narrower than the corresponding non-speed-dependent profiles. Similarly, most transitions show slightly greater shifts when fitted with Speed Dependent Voigt model. This study represents the first direct measurement of weak line mixing coefficients for the $30012 \leftarrow 00001$ and $30013 \leftarrow 00001$ bands. It can be seen that the values agree well with the EPG and ECS scaling law calculations.

Acknowledgments

Support for this project was provided by the Natural Sciences and Engineering Research Council of Canada, the University of Lethbridge Research Fund and the BIOCAP Foundation of Canada.

References

[1] M. Baranger, Phys. Rev. 111 (1958) 481–493.
[2] M. Baranger, Phys. Rev. 111 (1958) 494–504.
[3] M. Baranger, Phys. Rev. 112 (1958) 855–864.
[4] A.C. Kolb, H. Griem, Phys. Rev. 111 (1958) 514–521.
[5] R.F. Snider, J. Chem. Phys. 32 (1960) 1051.
[6] S.G. Rautian, A.M. Shalagin, Kinetic Problems of Nonlinear Spectroscopy, North-Holland, Amsterdam, 1991.
[7] L. Galatry, Phys. Rev. 122 (1961) 1218–1223.
[8] S.G. Rautian, I.I. Sobel'man, Sov. Phys. Usp. 9 (1967) 701–716.
[9] J. Keilson, J.E. Storer, Q. J. Appl. Math. 10 (1952) 243–253.
[10] P.R. Berman, J. Quant. Spectrosc. Radiat. Transfer 12 (1972) 1331–1342.
[11] J. Ward, J. Cooper, E.W. Smith, J. Quant. Spectrosc. Radiat. Transfer 14 (1974) 555–590.
[12] G. Nienhuis, J. Quant. Spectrosc. Radiat. Transfer 20 (1978) 275–290.
[13] V. Formisano, V. Cottini, M. Giuranna, D. Grassi, I. Khatuntsev, N. Ignatiev, A. Maturilli, G. Piccioni, B. Saggin, L. Zasova, Adv. Space Res. 36 (2005) 1074–1083.
[14] C.R. Webster, G.J. Flesch, K. Mansour, R. Haberle, J. Bauman, Appl. Opt. 43 (2004) 4436–4445.
[15] F.P.J. Valero, C.B. Suarez, J. Quant. Spectrosc. Radiat. Transfer 19 (1978) 579–590.
[16] C.B. Suarez, F.P.J. Valero, J. Mol. Spectrosc. 71 (1978) 46–63.
[17] M. De Rosa, C. Corsi, M. Gabrysch, D. D'Amato, J. Quant. Spectrosc. Radiat. Transfer 61 (1999) 97–104.
[18] J. Henningsen, H. Simonsen, J. Mol. Spectrosc. 203 (2000) 16–27.
[19] S.A. Tashkun, V.I. Perevalov, J.-L. Teffo, A.D. Bykov, N.N. Lavrentieva, J. Quant. Spectrosc. Radiat. Transfer 82 (2003) 165–196.
[20] C.E. Miller, L.R. Brown, J. Mol. Spectrosc. 228 (2004) 329–354.
[21] L.S. Rothman, D. Jacquemart, A. Barbe, D.C. Benner, M. Birk, L.R. Brown, M.R. Carleer, C. Chackerian Jr., K. Chance, V. Dana, V.M. Devi, J.-M. Flaud, R.R. Gamache, J.-M. Hartmann, K.W. Jucks, A.G. Maki, J.-Y. Mandin, S. Massie, J. Orphal, A. Perrin, C.P. Rinsland, M.A.H. Smith, R.A. Toth, J. Vander Auwera, P. Varanasi, G. Wagner, J. Quant. Spectrosc. Radiat. Transfer 96 (2005) 139–204.
[22] C.E. Miller, M.A. Montgomery, R.M. Onorato, C. Johnstone, T.P. McNicholas, B. Kovaric, L.R. Brown, J. Mol. Spectrosc. 228 (2004) 355–374.
[23] I. Pouchet, V. Zéninari, B. Parvitte, G. Durry, J. Quant. Spectrosc. Radiat. Transfer 83 (2004) 619–628.
[24] T. Hikida, K.M.T. Yamada, M. Fukabori, T. Aoki, T. Watanabe, J. Mol. Spectrosc. 232 (2005) 202–212.
[25] T. Hikida, K.M.T. Yamada, J. Mol. Spectrosc. 239 (2006) 154–159.
[26] S. Nakamichi, Y. Kawaguchi, H. Fukuda, S. Enami, S. Hashimoto, M. Kawasaki, T. Umekawa, I. Morino, H. Suto, G. Inoue, Phys. Chem. Chem. Phys. 8 (2006) 364–368.
[27] L. Régalia-Jarlot, V. Zéninari, B. Parvitte, A. Grossel, X. Thomas, P. von der Heyden, G. Durry, J. Quant. Spectrosc. Radiat. Transfer 101 (2006) 325–338.
[28] D. Boudjaadar, J.Y. Mandin, V. Dana, N. Picqué, G. Guelachvili, J. Mol. Spectrosc. 236 (2006) 158–197.
[29] R.A. Toth, L.R. Brown, C.E. Miller, V. Malathy Devi, D. Chris Benner, J. Mol. Spectrosc. 239 (2006) 221–242.
[30] R.A. Toth, L.R. Brown, C.E. Miller, V. Malathy Devi, D. Chris Benner, J. Mol. Spectrosc. 239 (2006) 243–271.
[31] V.M. Devi, D.C. Benner, L.R. Brown, C.E. Miller, R.A. Toth. J. Mol. Spectrosc. 242 (2007) 90–117.
[32] V.M. Devi, D.C. Benner, L.R. Brown, C.E. Miller, R.A. Toth, J. Mol. Spectrosc., in press, doi:10.1016/j.jms.2007.05.015.
[33] D. Hurtmans, G. Dufour, W. Bell, A. Henry, A. Valentin, C. Camy-Peyret, J. Mol. Spectrosc. 215 (2002) 128–133.
[34] A.R.W. McKellar, J.K.G. Watson, B.J. Howard, Mol. Phys. 86 (1995) 273–286.
[35] A.R.W. McKellar, Faraday Discuss. Chem. Soc. 97 (1994) 69–80.

[36] R. Ciurylo, A. Bielski, S. Brym, J. Jurkowski, J. Quant. Spectrosc. Radiat. Transfer 53 (1995) 493–500.
[37] A.S. Pine, J. Quant. Spectrosc. Radiat. Transfer 62 (1999) 397–423.
[38] A. Bielski, S. Brym, R. Ciurylo, J. Szudy, Eur. Phys. J. D 8 (2000) 177–187.
[39] C.B. Suarez, F.P.J. Valero, J. Quant. Spectrosc. Radiat. Transfer 43 (1990) 327–334.
[40] J.R. Drummond, A.D. May, R. Berman, S. Dolbeau, Spectral line shapes for atmospheric work: problems and solutions, Spectral Line Shapes, 10, College Park, PA, 1998.
[41] E.W. Smith, J. Chem. Phys. 74 (1981) 6658–6673.
[42] P.W. Rosenkranz, IEEE Trans. Antenn. Propag. 23 (1975) 498–506.
[43] A. Levy, N. Lacome, C. Chackerian Jr., in: K. Narahari Rao, A. Weber (Eds.), Spectroscopy of the Earth's Atmosphere and of the Interstellar Medium, Academic Press, New York, 1992, pp. 261–337.
[44] L.L. Strow, B.M. Gentry, J. Chem. Phys. 84 (1986) 1149–1156.
[45] D. Edwards, L.L. Strow, J. Geophys. Res.-Atm. 96 (1991) 20859–20869.
[46] B.M. Gentry, L.L. Strow, J. Chem. Phys. 86 (1987) 5722–5730.
[47] R. Berman, P. Duggan, P.M. Sinclair, A.D. May, J.R. Drummond, J. Mol. Spectrosc. 182 (1997) 350–363.
[48] A. Predoi-Cross, C. Luo, R. Berman, J.R. Drummond, A.D. May, J. Chem. Phys. 112 (2000) 8367–8377.
[49] T.A. Brunner, T.P. Scott, D.E. Pritchard, J. Chem. Phys. 76 (1982) 5641–5643.
[50] N. Smith, D.E. Pritchard, J. Chem. Phys. 74 (1981) 3939–3946.
[51] R. Rodrigues, K.W. Jucks, N. Lacome, Gh. Blanquet, J. Walrand, W.A. Traub, B. Khalil, R. Le Doucen, A. Valentin, C. Camy-Peyret, L. Bonamy, J.M. Hartmann, J. Quant. Spectrosc. Radiat. Transfer 61 (1999) 153–184.
[52] A. Predoi-Cross, A.D. May, A. Vitcu, J.R. Drummond, J.-M. Hartmann, C. Boulet, J. Chem. Phys. 120 (2004) 10520–10529.
[53] F. Niro, C. Boulet, J.-M. Hartmann, J. Quant. Spectrosc. Radiat. Transfer 88 (2004) 483–498.
[54] A.E. DePristo, S.T. Augustin, R. Ramaswamy, H. Rabitz, J. Chem. Phys. 71 (1979) 850–865.
[55] Available from <http://library.wolfram.com/infocenter/MathSource/5344/>.